NEUTRINO INTERACTIONS IN EMULSION STACKS INSIDE THE FERMILAB 15-FOOT BUBBLE CHAMBER

THE FERMILAB E-564 COLLABORATION

W. SMART AND L. VOYVODIC

Fermi National Accelerator Laboratory, Batavia, IL 60510, USA

H. RUBIN

Illinois Institute of Technology, Chicago, IL 60616, USA

V. AMMOSOV, V. BARANOV, V. GAPIENKO, V. KLYUKHIN, V. KORESHEV, P. PITUKHIN, V. SIROTENKO, E. SLOBODYUK AND V. YARBA

Institute of High Energy Physics, Serpukhov, USSR

A. JURAK, A. OLSZEWSKI, B. WILCZYŃSKA, H. WILCZYŃSKI, W. WOLTER AND B. WOSIEK

Institute of Nuclear Physics, Cracow, Poland*

M. IVANOVA AND H. TCHERNEV

Institute of Nuclear Research, Sofia, Bulgaria

O. EGOROV, P. GORITCHEV, E. KOLGANOVA, I. MAKHLYUSHEVA, E. POZHAROVA, V. SHAMANOV, V. SHEVCHENKO, V. SMIRNITSKY AND A. WEISSENBERG†

Institute of Theoretical and Experimental Physics, Moscow, USSR

YU. BATUSOV, S. BUNYATOV, O. KUZNETSOV, V. LYUKOV AND V. TRETYAK

Joint Institute for Nuclear Research, Dubna, USSR

* Address: Instytut Fizyki Jądrowej, Zakład V, Kawiory 26a, 30-055 Kraków, Poland.
† Deceased.

R. AMMAR, D. COPPAGE, R. DAVIS, J. GREES, N. KWAK, R. RIEMER AND R. STUMP

University of Kansas, Lawrence, KS 66045, USA

A. BAKICH AND L. PEAK

University of Sydney, Sydney, Australia

T. BURNETT, S. KRZYWDZIŃSKI, J. LORD, R. ROSENBLADT AND R. WILKES

University of Washington, Seattle, WA 98195, USA

(Received April 17, 1985)

We report a study of neutrino interactions on heavy nuclei in an exposure of emulsion stacks placed inside the Fermilab 15-foot Bubble Chamber. Our technique for locating interactions in cryogenically sensitive emulsions using bubble chamber measurements is described. We have compared hadrons produced in 128 charged-current neutrino interactions selected from 294 interactions found in emulsion, with hadrons produced in neutrino-deuterium interactions in the bubble chamber liquid. We have located and analyzed 5 charm particle decays.

PACS numbers: 13.15.-f

1. Introduction

The properties of production and decay of charmed particles are crucial to tests of current models of strong and electro-weak interactions. Recently several experiments have been performed using nuclear emulsions [1–9], streamer chambers [10], bubble chambers [11, 12], and silicon detectors [13] to observe the weak decays of charmed particles.

Nuclear emulsion offers a higher effective target mass ($\langle A \rangle \sim 80$) than other track-sensitive targets, and its fine spatial resolution, of the order of 1 μm, is ideally suited to detect weak decays of charmed particles with lifetimes of the order of 10^{-13} to 10^{-12} sec. The use of emulsions alone to detect rare processes is not practical because of the prohibitive scanning effort required. However, in a hybrid system where an emulsion is used as a primary vertex detector in conjunction with a fine-grained downstream detector for secondary tracks, it is possible to:

(a) use the signature of the event in the downstream detector to locate the interaction vertex in the emulsion, thus reducing substantially the emulsion scanning time;

(b) identify and measure the momenta of charged secondaries;

(c) detect and measure some of the relatively long-lived neutral component of the interaction.

An emulsion exposure in a neutrino beam is most favorable for exploiting this technique because non-interacting neutrinos do not produce massive backgrounds in the emulsion

and the yield of charmed hadrons from charged-current neutrino interactions is relatively high, of the order of 5 to 10% [5, 14]. In addition, the interaction parameters involved are better defined than in the case of incident hadrons or photons, since the four-momentum transferred to the target can be determined directly from the observed interaction products. On the other hand, due to the very small neutrino interaction cross section, large emulsion volumes and/or long exposure times (up to 3 to 4 months) are required to acquire a substantial event sample. This can lead to backgrounds in the emulsions from cosmic rays and charged particles normally found in the environment of a large accelerator beam line.

Such a hybrid technique to search for charmed particle decays in neutrino interactions was successfully employed for the first time at Fermilab [1]. In addition, nuclear emulsions have been used as external targets with bubble chambers and electronic detectors in muon [2] and neutrino [3–6, 8, 9] beams at Fermilab, CERN, and Serpukhov.

In the present experiment, cryogenically sensitive BR2 emulsions were placed inside the Fermilab 15-foot bubble chamber. By placing emulsions inside a bubble chamber, the solid angle coverage of the chamber is maximized, while the distance and amount of matter between the emulsion target and chamber liquid is minimized. These advantages are gained at some cost, however: the emulsions used must be sensitive at cryogenic temperatures, and access to the emulsion stacks during exposure is limited.

Two neutrino exposures were carried out, with 20 liters of emulsion irradiated in each run. We present here a description of the experimental techniques employed and a summary of our results.

2. Experimental apparatus

2.1. Cryogenically sensitive emulsion

Normal nuclear emulsions lose from about 70 to 100% of their initial sensitivity to charged particles at liquid hydrogen temperature. Therefore, special cryogenically sensitive BR2 emulsions were prepared for this experiment. This was accomplished by the elimination of iodine which causes fluorescence at low temperatures [15]. The elimination of iodine also increases the electron trapping efficiency of the silver halide crystals, and these trapped electrons act as a prelatent image while the conventional latent image is formed when increased temperature allows greater ionic mobility.

However, an undesirable side effect of the low temperature sensitivity is that the emulsion is susceptible to rapid fading at high temperature. Test measurements of this fading were done during exposures for each of the 9 emulsion batches produced (4 for the first run and 5 for the second). Samples were irradiated and stored for various lengths of time (up to 24 weeks) at $+20°C$, $+5°C$, and $-10°C$ before development, with the result that production emulsions were stored at or below $+5°C$ between exposure and development. This handling resulted in retention of 70 to 75% of the initial sensitivity. The absolute density measured for relativistic tracks in events was 21 to 29 grains/100 μm in the first run, and 34 to 37 grains/100 μm in the second, with somewhat higher background fog levels than in conventional emulsions ($\gtrsim 2$ grains/1000 μm^3).

2.2. The emulsion target structure

For each run, the emulsion pellicles were prepared at the State Institute of Photochemical Industry in Moscow and thenas sembled at Serpukhov in 22 separate stacks. Each stack consisted of about 200 pellicles with nominal thickness of 400 to 500 μm, and area 4.6 by 19.2 cm^2. The total volume of emulsion in a single stack was 0.9 liters. A total of 9220 pellicles were used in the two runs.

During the target assembly, the stacks were clamped and the stack surfaces were milled flat and perpendicular to one another. Then a special tool was used to scribe one of the 10 by 19 cm^2 faces of each stack with vertical and diagonal lines. These scribe marks left notches on each pellicle which were readily visible after processing, thus permitting accurate determination of the location of each pellicle despite inevitable non-uniformities in pellicle thickness. Following milling and scribing, each stack was painted with gelatin to help maintain a solid block structure after their removal from machining clamps. The stacks were then measured, wrapped, and shipped by air to Fermilab.

2.3. The emulsion installation

The location of the emulsions inside the 15-foot bubble chamber is shown in Fig. 1. The emulsions were placed in two stainless steel boxes which were mounted on the 15-foot chamber nose cone flange just above and below the median plane of the chamber. This location of the emulsion boxes made it possible, by "conventional" scanning of the bubble chamber film, to identify events likely to have resulted from neutrino interactions in the emulsion. A bubble chamber picture containing a candidate emulsion event is reproduced in Fig. 2.

Each emulsion container had exterior dimensions of 28 cm by 152 cm by 10 cm, and

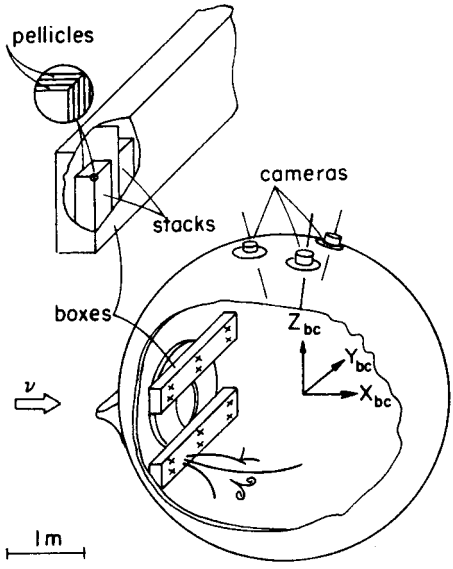

Fig. 1. Location of emulsion stacks inside the Fermilab 15-foot Bubble Chamber

was divided into 11 cells by stainless steel retaining walls. The beam entry and exit walls and cell separators were 1/4-inch thick. Three spring-loaded panels were used to press each emulsion stack against a downstream corner of its cell. This corner formed the origin of the cell coordinate system. The positions of the reference walls of each cell were accurately measured (± 0.005 cm) relative to external fiducials scribed on the outside front and top faces of each box. These fiducials formed the basis of transformations from bubble chamber coordinates to emulsion cell coordinates.

The stacks were placed so that the pellicles were parallel to the $X-Z$ bubble chamber plane, with the small dimension (4.6 cm) along the beam direction (the bubble chamber X-direction). Several factors influenced this choice of emulsion orientation. Previously it had been found that multiple scattering limits the efficiency of finding tagged events more than about 5 cm into an emulsion stack. The accuracy in vertex position transverse to the beam direction is better by a factor of 2 in the horizontal (Y) direction than in the vertical (Z) direction due to the bubble chamber camera configuration; there is also less liquid motion in the horizontal direction. Pellicles were therefore oriented perpendicular to the Y-direction since emulsion scanning within one pellicle is easier than scanning an equivalent volume in several pellicles.

2.4. Exposure and processing

Two emulsion exposures were carried out in the Fermilab wide-band neutrino beam at incident proton energies of 350 and 400 GeV respectively. In both runs, the neutrino energy spectrum peaks at about 15 GeV, and extends to about 200 GeV.

In the first run, during the winter of 1978–79, the bubble chamber was filled with liquid deuterium, and 315000 pictures were taken with a total of 5×10^{18} protons on target, with 75% of these pictures available for emulsion candidate analysis. In the second run, in 1980–81, the bubble chamber was filled with a heavy neon-hydrogen mixture (64%-atomic neon), and 280000 pictures were taken with 3.3×10^{18} protons on target. From the measured event rates in the bubble chamber, we estimate that about 870 charged-current neutrino interactions should have occurred within the emulsion fiducial volume.

To avoid rapid fading after exposure, the emulsion was kept at 0°C by packing them in dry ice and was shipped by air to the USSR for processing. Prior to development, 1 mm coordinate grids were printed on the surface of each pellicle, the thickness of each pellicle was measured, and the pellicles were mounted on uniformly sized glass plates.

In both runs, the time from emulsion manufacture to development was about 6 months, leading to rather large expected backgrounds. From an examination of the bubble chamber pictures, we estimate the beam-associated background to be about 3 particles/mm^2 for the entire run. The total background was about 100 particles/mm^2 in a cone ± 20 degrees about the beam direction.

3. Event search procedure

Due to the hybrid nature of the experiment, the search for events naturally divided into two phases. First, bubble chamber events were selected and processed, resulting in predictions for interaction vertices within the emulsion target. Second, an emulsion scan

TABLE I

Event statistics

Number of:	Run 1	Run 2	Total
BC pictures scanned	237000	280000	517000
events selected and measured	2800	3300	6100
total predictions	1140	1340	2480
"good" predictions	700	600	1300
events scanned in emulsion	930	700	1630
found events	90	194	284
neutrino interactions	51	102	153
charged current events	43	85	128
decay candidates	2	3	5

was carried out for events with track configurations matching the bubble chamber topologies. The essential features of each step are described here. The event statistics are summarized in Table I.

3.1. Bubble chamber film analysis

The bubble chamber film was scanned for events with tracks apparently emerging from a common point inside the emulsion target. The event selection criteria required a minimum of 2 such tracks; at least 1 of these was to have a momentum of greater than 1 GeV/c and an angle of less than 30 degrees with respect to the beam direction. The average scanning yield was about 1 event per 30 scanned frames.

The selected event sample was then edited in an effort to provide early rejection of spurious events. A number of editing schemes were used, each involving some form of visual estimate of the likely location of the tracks' convergence point. In the approach finally adopted, the visually estimated vertex point was digitized and a preliminary reconstruction was performed while the event was on the scan table. The event was rejected if the estimated vertex location was outside the emulsion target boundaries. The editing process reduced the number of selected events to about 1 in 85 frames, resulting in a total of 6100 emulsion event candidates.

These event candidates were then conventionally measured in three views, and duplicate film copies were made [8] to enable further remeasurements after the original film was returned to the prime users (Fermilab experiments E-545 and E-53). For each event, the tracks were measured as one-prongs with vertices at the first visible point on the face of the emulsion box. From the measurement data the tracks were reconstructed using either TVGP [16] or HYDRA-based [17] geometry programs, depending on the laboratory in which measurements were made.

3.2. Vertex prediction

Several programs were used for predicting the event vertex location from the geometry output data [8, 18, 19]. Although substantially different mathematical methods were employed by these programs, the results were generally consistent and provided a very

useful check of the credibility of the predicted vertices. The program which provided most predictions for the second run is briefly described here [18].

This vertex reconstruction program made two successive approximations to determine the best vertex location. During the first step, all reconstructed tracks, vees and gammas with momentum greater than 0.2 GeV/c and with fractional error less than 30%, were extrapolated upstream. In extrapolating tracks, curvature due to the magnetic field and ionization losses were taken into account. The tracks were then combined into apparently converging groups called multiples, thus allowing for possible secondary vertices (whether of hadronic or electromagnetic origin) and rejecting obviously unassociated background tracks. Pairs of tracks (doubles) with distances of closest approach less than 3 mm were selected first. For a track to qualify as a member of a higher multiple, its distance of closest approach to a midpoint (weighted by the propagated measurement errors) of every double contributing to the multiple, had to be less than 5 mm. Any non-participating track was rejected as unassociated. A centroid of such a convergent multiple of tracks was taken as the first approximation to the vertex location. The parameters of the tracks extrapolated to a reference plane located at the first vertex approximation and the coordinates of this first approximation were then used as input to the second vertex fit.

The second and final vertex fit was obtained by minimizing the sum of squares of the deviations (expanded in terms of small arc length variations) of the tracks' starting points from the assumed vertex position. The vertex position was then updated and the procedure was iterated until arc length variations were reduced to below 1 mm, or until 20 iterations were done. The algorithm of the fit was very close to the CONVEX procedure in HYDRA geometry [17].

A set of fiducials marked on the outside surface of each emulsion box was used to transform predictions into the coordinate system of the appropriate emulsion cell. In the first run, bubble chamber coordinates of 6 fiducials on each box, averaged over a large number of measurements on film, were used together with their survey measurements to produce a 6-parameter transformation for all events. In the second run, 20 fiducials on each box were measured and a 12-parameter transformation was calculated for each event individually.

For the sample of 6100 measured events, the vertex reconstruction efficiency (at least one vertex reconstructed) was found to be about 80%; approximately half of the reconstructed events were found to be outside the emulsion target. The resulting sample of 2480 events had at least one vertex within the emulsion.

3.3. Quality of bubble chamber data

For each event, the final output of the bubble chamber data analysis consisted of the predicted vertex location and the fitted track parameters. In an attempt to assess the quality of this data, a sample of 400 events was remeasured several times and reprocessed using the same set of 3 views and the same geometry and prediction programs.

The results of this procedure are presented in Figs. 3 and 4. The RMS uncertainties of track coordinates at the downstream face of the emulsion stack show an obvious momentum dependence due primarily to multiple scattering in the box walls, approaching

0.5 mm in the horizontal direction for high momentum tracks. The uncertainties in track angles show similar behavior, with accuracies better than ± 0.5 deg for high momentum tracks.

With respect to the accuracy of the crucial vertex prediction, we note from Figs. 5 (a) and (b) that the errors appear to flatten out to acceptable values for higher fit multiplicity events ($N_{\text{fit}} > 4$). However, for $N_{\text{fit}} \leqslant 4$ the vertex predictions are very poor, especially in the beam direction.

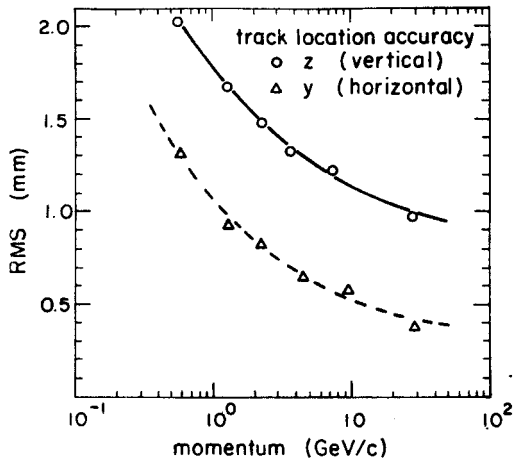

Fig. 3. Bubble chamber measurement accuracy of track coordinates versus momentum dependence. The accuracy is given for the two coordinates, Y, Z, transverse to the beam, after extrapolating the bubble chamber tracks to the downstream face of an emulsion stack (fixed X location) and includes the transformation to the emulsion box system

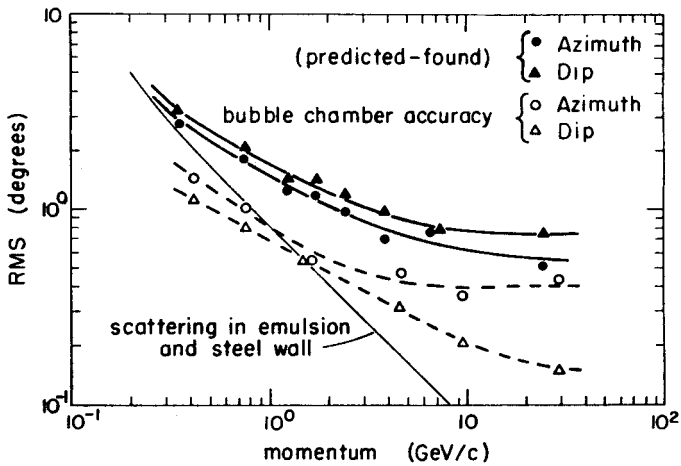

Fig. 4. Bubble chamber measurement accuracy of track angles (open symbols) and the difference between predicted and found angles (filled symbols) versus momentum dependence. The angles are given in emulsion convention; the transformation of angles from the bubble chamber to emulsion corresponds approximately to an azimuth (— — —) dip interchange

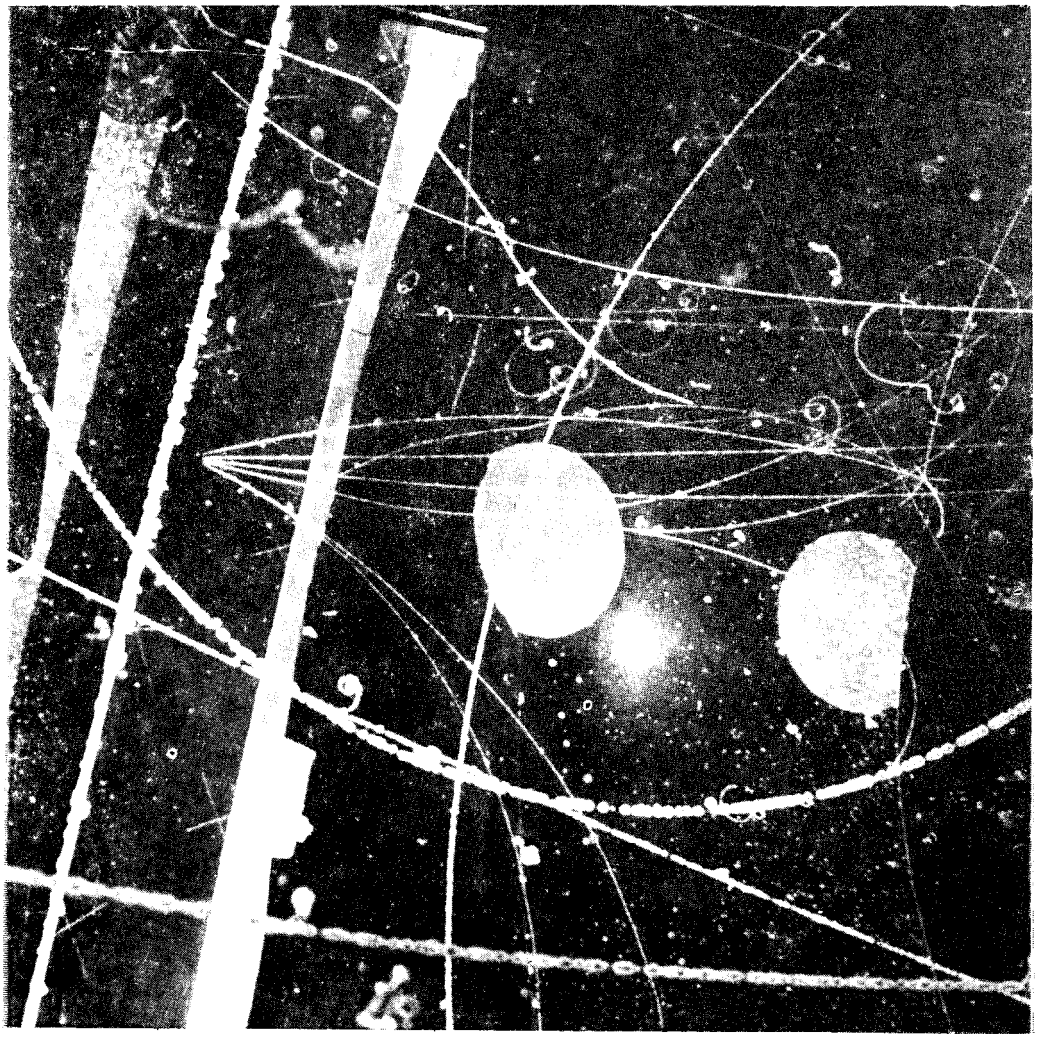

Fig. 2. A bubble chamber picture with an emulsion event candidate

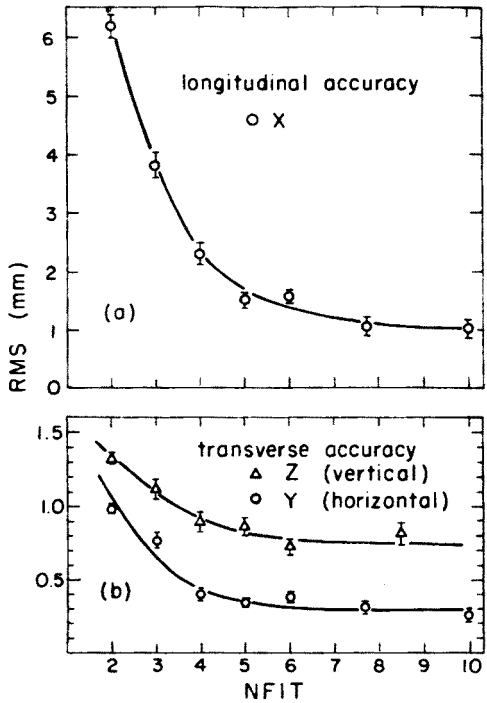

Fig. 5. Vertex prediction accuracy versus the number of tracks entering into the vertex fit; only fits consisting of the same tracks but resulting from independent measurements of an event were compared to estimate the accuracy: (a) location along the beam; (b) location transverse to the beam

TABLE II

Average BC accuracy (RMS) of track parameters and vertex predictions

	$\langle N_{fit} \rangle$	ΔX (mm)	ΔY (mm)	ΔZ (mm)	ΔDip (deg)	ΔAzim (deg)
Tracks at emulsion face	—	—	1.00	1.69	0.70	0.88
Vertices: $N_{fit} > 1$	3.9	4.25	0.73	1.09	—	—
Vertices: $N_{fit} > 2$	5.0	2.60	0.53	0.93	—	—

The results are summarized in Table II, where the average values of the errors were estimated by folding in appropriate momentum and track multiplicity distributions.

In an attempt to improve accuracy and to produce a single prediction, all available remeasurements of an event were usually combined and averaged before passing them through the prediction program.

3.4. Emulsion scanning procedure

In order to preselect events suitable for scanning, three cuts were imposed on the preliminary sample of 2480 predicted events. Each "good" candidate was required

(a) to have a vertex location well defined by either a unique prediction or by closely spaced predictions corresponding to different "multiples" (as defined in Sec. 3.2),

(b) to have at least 3 fitted tracks,

(c) to be located at least 1 standard deviation within the emulsion volume.

These selection criteria were satisfied by 1300 events.

For each event the cold-cell vertex coordinates were transformed into a pellicle number and a 1-mm-square grid coordinate system. For determining the required pellicle, both premeasured pellicle thickness data and up to five scribe mark notches on the reference edge (at the downstream stack face) of the pellicles were used. The grid location of the event was then determined by allowing for measured grid offsets with respect to the reference edges of the stack. This transformation took into account thermal shrinkage and the wrapping of the emulsion stacks.

Most of the predictions were volume-scanned under a magnification of about 250. A scanning volume, centered on the predicted vertex position, was extended for at least ± 2 standard deviations in each of the three coordinates. This typically corresponded to ± 5 mm in the beam direction and ± 2.5 mm by 7 pellicles perpendicular to the beam, or a total scanning area of 350 mm^2. Any star located within this volume with a number of heavily ionizing tracks was examined under high magnification (1000) for the presence of any shower tracks. The event was then accepted if the angles of at least two shower tracks could be matched to within 2 degrees of any of the bubble chamber tracks. This volume-scanning method was very inefficient for finding events with a low number of heavily ionizing tracks (N_h). Test scans indicated that while the scanning efficiency was about 75% for $N_h > 2$, it was as low as 20% for $N_h = 2$.

For two stacks from the second run, an attempt was made to assess the possibility of using a track-following technique [5, 9]. Since, as mentioned above, the accuracy of the track exit point coordinates was relatively poor (± 1 mm) compared to the matching precision of the track angles (better than ± 0.7 degrees for tracks above 1 GeV/c), the following procedure was adopted. First, a high magnification scan for any minimum ionizing tracks with the predicted angles (± 2 degrees) was made at an appropriate fixed distance (about 10 mm) downstream from the predicted vertex. Then the best selected tracks were followed upstream well past the predicted vertex position. The event-finding efficiency of this technique was $\sim 50\%$, and 11 events of the 32 found in these two stacks were located by this technique. Although obviously independent of N_h and less sensitive to the low prediction accuracy in the beam direction, the usefulness of this technique was limited by the relatively high count of background tracks (almost entirely due to cosmic rays) of about 1 track per mm, per pellicle, per ± 2 degrees angle bin.

4. Event search results

4.1. Event detection efficiency

A total of 1630 events were scanned. This included the 1300 good predictions, defined by at least 3 fitted tracks and located within the emulsion fiducial volume, and in addition, about 15% of the poorer predictions with either 2-track fits or very close to the emulsion edge.

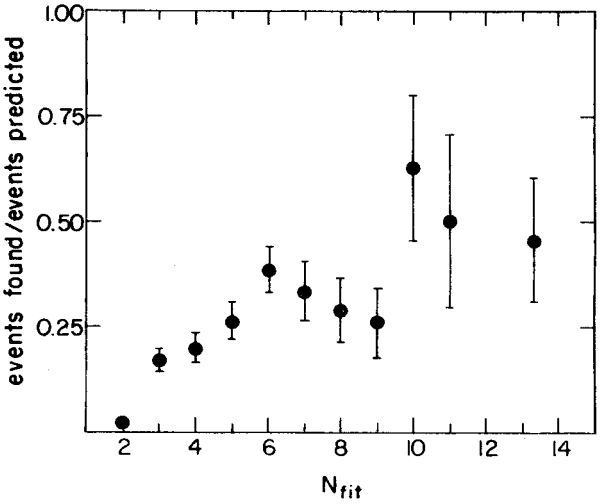

Fig. 6. Ratio of the number of events found to the number of events predicted versus the number of tracks in the vertex fit. The data shown include only that fraction of second run events predicted by the program EMPRED [18]

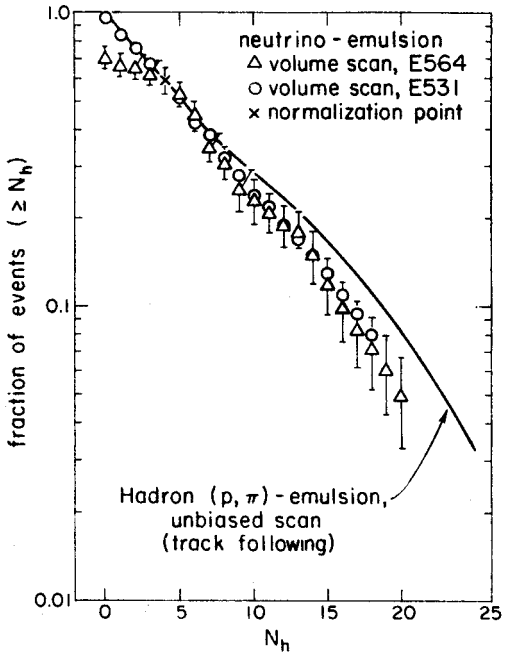

Fig. 7. Integral N_h distribution. Neutrino-emulsion data from this experiment (E-564) is compared with E-531 data [5, 18] obtained by volume scanning. Hadron (proton, pion) — emulsion data [2, 20] at energies ranging from 60 GeV to 300 GeV is also shown. For hadron data, the vertical scale gives the actual fraction of events, whereas neutrino data samples were normalized at $N_h = 4$

284 events were found. For the sample of good predictions only, this corresponds to an event-detection efficiency of about 22%. We note that this figure represents an average of 13% for the first run, and 32% for the more successful second run, as indicated in Table I. These results can best be understood by considering the two factors most likely to affect the search efficiency.

(a) Considering the bubble chamber data processing, we note that the uncertainty in the predicted vertex location increases significantly for low multiplicity of fitted tracks, as shown in Fig. 5. Because there is relatively little redundant information contributing to the fit, these low-N_{fit} events are also particularly susceptible to a further reduction in the reliability of predicted vertex locations resulting from scattering and interactions both in the emulsion and in the emulsion box walls. The decrease in the event-detection efficiency for low N_{fit} events can be seen in Fig. 6.

(b) During the emulsion search, the volume-scanning method was very inefficient for finding events with low numbers of heavily ionizing tracks, as discussed in the previous section. Since in this experiment the track following technique was used only on a limited trial basis, one would expect substantial losses of low-N_{h} events. By neglecting losses due to large prediction uncertainties for events with $N_{\mathrm{fit}} > 5$, we estimate from Fig. 6 that about 50% of the events were lost due to the low-N_{h} scanning efficiency. This estimate can be confirmed by comparing our integral N_{h} distribution with high-statistics unbiased (track following) scan data from hadroproduction experiments [2, 20], as shown in Fig. 7. The N_{h} distributions agree within errors for $N_{\mathrm{h}} > 4$, and the deviation for $N_{\mathrm{h}} \leqslant 4$ is consistent with our estimate of finding efficiency for high N_{fit} events, as shown in Fig. 6. The results are also consistent with volume scan data from another neutrino experiment employing a different exposure technique [5, 9].

4.2. Predicted *vs* found comparison

For the 284 found events a detailed comparison between the bubble chamber and emulsion data was made. The distributions of the differences between the predicted and found vertex positions are presented in Fig. 8.

There appears to be no significant systematic bias, except for the Z-coordinate. The exact reason for this shift is not clear; one possibility is that this vertical displacement results from bubble rise during the flash delay.

The RMS spreads of the distributions reflect the overall resolution accuracy of the entire event-search process, from the bubble chamber measurements through to the final transformation of the predicted vertex locations into the grid-pellicle system of the emulsion stacks, as described in Section 3. Comparing these effective RMS values with the bubble chamber vertex prediction uncertainties estimated above (see Fig. 5 and Table II, $N_{\mathrm{fit}} > 2$ entry), we find that whereas the spread in the beam direction can be easily accounted for, there exists a significant additional widening in both transverse coordinates. A detailed analysis of this extra spreading suggests that it is due mainly to the use of different vertex prediction programs and stack-dependent transformations by different laboratories. Using results from a single prediction program [18] and found events to correct stack calibrations,

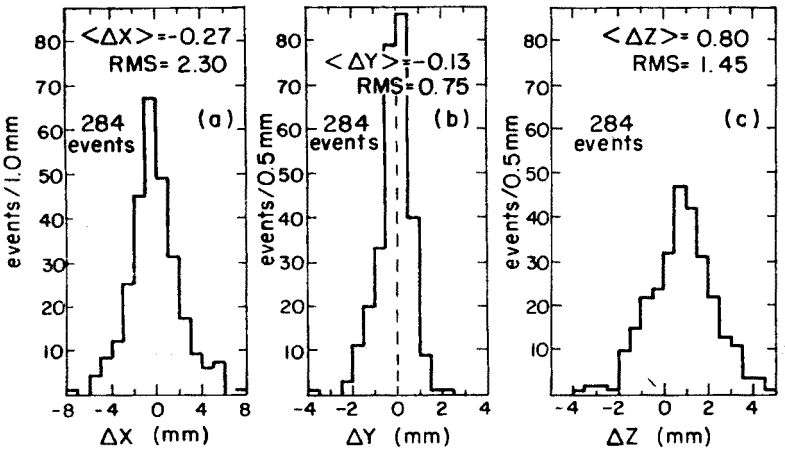

Fig. 8. Differences between predicted and found vertex positions: ΔX — along the beam, ΔY, ΔZ — transverse to the beam (horizontal and vertical differences respectively)

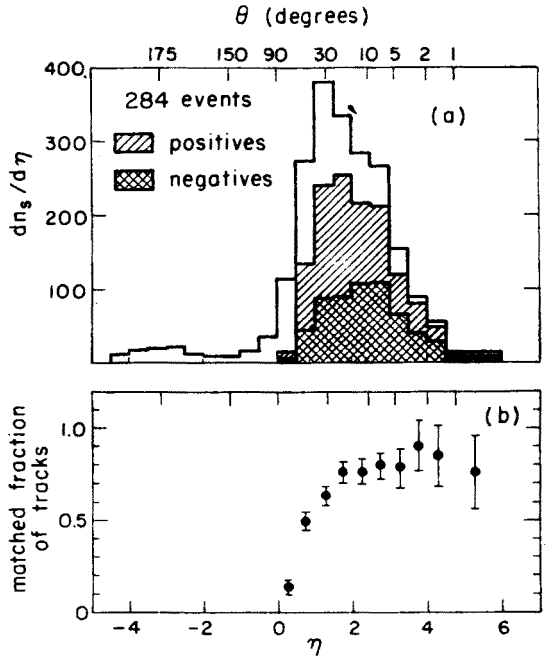

Fig. 9. (a) Pseudorapidity distribution of shower tracks; shaded areas indicate shower tracks matched with bubble chamber tracks. (b) The fraction of matched tracks. Pseudorapidity/angle is calculated relative to the neutrino direction

(a linear transformation between predicted and found locations was applied separately for each stack with more than 7 events found) one arrives at an estimate of overall vertex prediction accuracy: $\Delta X = 2.1$ mm, $\Delta Y = 0.6$ m, and $\Delta Z = 1.1$ mm.

A special program matching emulsion and bubble chamber tracks yielded 63% matches of shower tracks and 9% matches of grey tracks; almost all matches of grey tracks (> 94%) were positively charged tracks. Fig. 9 shows the angular distribution of all shower tracks and their matched fraction; for angles up to 30 degrees the fraction is about 80%, but then drops toward zero at 90 degrees.

The momentum dependence of the difference between predicted and found angles for the matched tracks is shown in Fig. 4. At high momenta the difference can be accounted for by measurement errors in the bubble chamber and emulsion; at low momenta (< 1 GeV/c), the difference is dominated by the multiple Coulomb scattering in emulsion and in the steel wall of the emulsion box.

4.3. Event analysis

The 284 found events were analyzed in an effort to select the charged-current neutrino interactions.

Since in this experiment the bubble chamber environment prevented the implementation of a veto anti-coincidence system, events with charged incoming tracks were eliminated by imposing a cut on the angle relative to the assumed neutrino beam direction of any "backward" minimum-ionizing track with $p\beta > 1$ GeV/c. From a study of the angular distribution of such tracks, this cut was set at 165 degrees, rejecting 75 events (26 %).

The charged-current neutrino interactions were selected by means of a combination of kinematic cuts. First, the muon candidate was selected as the highest-transverse-momentum track (relative to the neutrino beam direction) among the tracks matched and leaving the bubble chamber with no interaction; in addition its longitudinal momentum was required to be > 2 GeV/c. Fifty-six event candidates (20%) were rejected because they contained no muon candidate according to these criteria. Extensive Monte-Carlo studies carried out on the larger samples of bubble chamber events in hydrogen [21] and in the deuterium experiment of the first run [22], and verified using the External Muon Identifier (EMI), indicate that this procedure correctly identifies the muon in 95% of all charged -current interactions. It has been noted in previous bubble chamber experiments that there can be substantial background from non-charged-current neutrino interactions introduced by using this kinematic muon identification. To reduce this background additional tests of the muon candidate relative to the charged hadron system are generally made. The total momentum of all matched shower tracks excluding the muon candidate was calculated; tracks interacting or decaying in the emulsion whose momenta could be determined from measurements of their secondaries in the bubble chamber were also included in this sum. The transverse momentum of the muon candidate relative to the estimated visible hadron system direction was required to be > 1 GeV/c. An additional 25 events (9%) were thus rejected. Monte-Carlo studies [22] indicate that fewer than 5% of background events

(neutral hadron secondary interactions, electron-neutrino events and neutral-current events) remain after this transverse momentum cut.

The remaining sample of 128 events (121 μ^- and 7 μ^+) was assumed to be due to charged-current neutrino interactions. Taking into account the average event-detection efficiency of 22%, some 165 neutrino interactions should have been found. This discrepancy can only be explained by the inefficiency of the vertex reconstruction procedure and the bubble chamber event selection for low-multiplicity events. Some evidence of the latter effect was apparent in the systematic dependence of the number of predicted events on the location of a stack in the target assembly. Also, muons in some high-multiplicity and cascading events, particularly in the neon-hydrogen mixture of the second run, may have been unmeasurable, thus depleting the final sample.

4.4. Kinematic parameters of the charged-current sample

In addition to the measurable "visible" energy, $E_{\text{vis}} = P_{\text{l}}^{\mu} + P_{\text{l}}^{\text{H}}$, a variety of calculations have been used to estimate the total neutrino energy from the observed muon and hadron momenta [21, 23–25]. $\vec{P}^{\mu}$ and $\vec{P}^{\text{H}} = \Sigma \vec{p}^{\text{H}}$ denote the muon momentum and the vector sum of the momenta of the other charged particles, respectively. (For emulsion events, only tracks which are matched in the bubble chamber are included in the hadron summation.) We used a variation of the Heilemann method [24], where the neutrino energy is given by:

$$E_{\nu} = P_{\text{l}}^{\mu} + P_{\text{l}}^{\text{H}}(1 + |\vec{P}_{\text{t}}^{\mu} + \vec{P}_{\text{t}}^{\text{H}}|/\Sigma\,|\vec{P}_{\text{t}}^{\text{H}}|).$$

The method assumes that the charged and neutral hadron systems are emitted at the same angle relative to the neutrino direction.

We use conventional definitions for the relevant kinematic variables:

$Q^2 = 4E_{\nu}E_{\mu}\sin^2(\theta_{\mu}/2)$	four-momentum transfer squared,
$x = Q^2/2M(E_{\nu} - E_{\mu})$	Bjorken x,
$y = (E_{\nu} - E_{\mu})/E_{\nu}$	hadronic inelasticity,
$W^2 = 2M(E_{\nu} - E_{\mu}) + M^2 - Q^2$	hadronic c–m energy squared,
$\eta = -\ln\tan(\theta_{\text{H}}/2)$	hadron pseudorapidity,

where M is the nucleon mass, θ_{μ} is measured relative to neutrino beam, and θ_{H} is measured relative to the hadronic system direction.

4.5. Nuclear effects

Lepton-nucleus interactions provide an important source of information regarding the space-time development of multiparticle production on nuclei. In contrast with hadroproduction, intranuclear cascading can be studied without the complicating effects of projectile rescattering or overlapping interactions of multiple projectile constituents [26]. Several models have been developed which directly address leptoproduction and permit testing of hypotheses relevant to models of hadroproduction [27–35].

In a study of the influence of heavy emulsion targets on the hadronic system produced in neutrino interactions, a comparison was made of the emulsion data with isoscalar deuterium data obtained in the bubble chamber exposure during the first run [36]. For this comparison, the deuterium sample was selected using the same kinematic cuts (see Sec. 4.3) and the same method was used to calculate the neutrino energy (see Sec. 4.4). In addition, to further reduce biases resulting from different procedures used in acquiring the data in the bubble chamber and emulsions, several other cuts were applied to both samples: $E_{vis} > 5$ GeV, $E_\nu > 10$ GeV, neutrino energy correction < 3, and the multiplicity of shower ($\beta > 0.7$) hadron tracks $n_s^H = n_s - 1 > 2$. These cuts introduce biases in both the deuterium and emulsion charged-current samples, and we have not attempted to correct for these biases. However, careful studies of the two samples as a function of the cuts

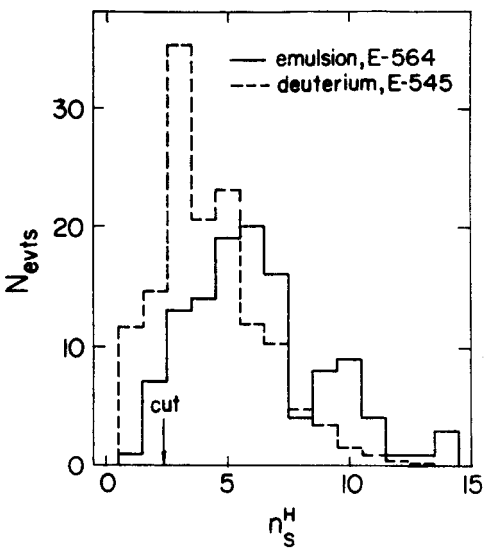

Fig. 10

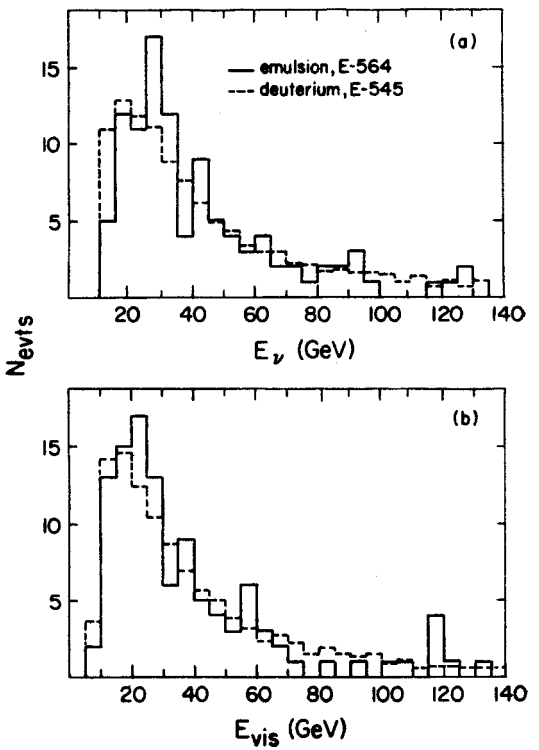

Fig. 11

Fig. 10. Multiplicity distributions of shower ($\beta > 0.7$) hadron tracks, n_s^H, for ν-Emulsion and ν-Deuterium interactions. The two distributions are normalized to the number of events in emulsion with $n_s^H > 2$. The ν-D_2 data is from Fermilab experiment E-545 [36]. Note that the plots do not represent unbiased charged--current distributions because of the cuts on the data described in Secs. 4.3 and 4.4

Fig. 11. Comparison of ν-Em with ν-D_2 samples, normalized to emulsion data. (a) Estimated neutrino energy E_ν, (b) visible neutrino energy E_{vis}. The ν-D_2 data is from Fermilab experiment E-545 [36]. Note that the plots do not represent unbiased charged-current distributions because of the cuts on the data described in Secs. 4.3 and 4.4

applied indicate that whatever biases might be introduced have little effect on the relative shapes of the distributions presented below, and in particular on the characteristics of the produced hadronic systems. Distributions of the hadron multiplicity and some of the kinematic variables are shown for both samples in Figs. 10 through 12; average values of the variables are compared in Table III where the errors quoted are statistical only. The comparison reveals no significant differences in the two samples with respect to the lepton vertex. Therefore it is reasonable to attribute differences between the produced hadronic systems

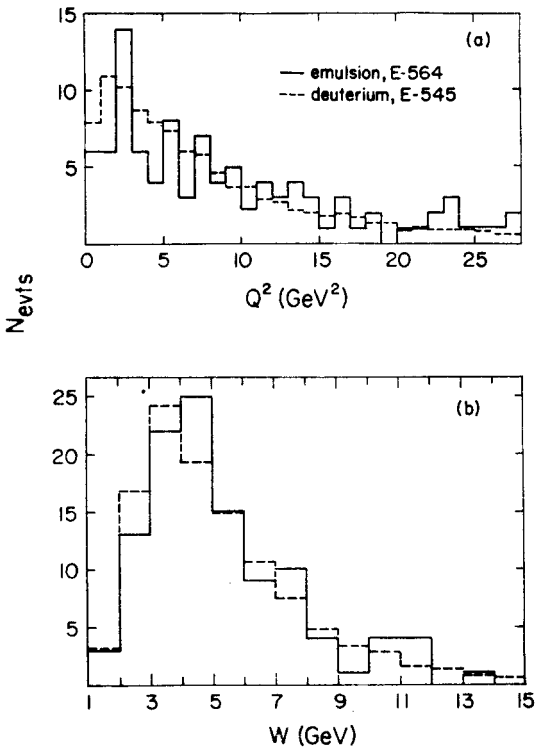

Fig. 12. Comparison of ν-Em with ν-D_2 samples, normalized to emulsion data. (a) Four-momentum transfer squared Q^2, (b) hadronic center of mass energy W. The ν-D_2 data is from Fermilab experiment E-545 [36]. Note that the plots do not represent unbiased charged-current distributions because of the cuts on the data described in Secs. 4.3 and 4.4

to the different targets used. From the data of Fig. 10, the overall multiplicity ratio calculated for events with $n_s^H > 2$ is, again with a statistical error,

$$R_\nu = \langle n_s^H \rangle_{\nu-Em} / \langle n_s^H \rangle_{\nu-D_2} = 1.32 \pm 0.05.$$

Our value of R_ν appears to be smaller than a similar ratio measured at somewhat higher energy ($W \approx 11$ GeV) for emulsion interactions of hadrons ($R_p = 2.53 \pm 0.07$, $R_\pi = 2.10 \pm 0.10$) and possibly to that found for muons ($R_\mu = 1.59 \pm 0.12$) [2, 20, 37]. The muon value was calculated over a different range of variables at the lepton vertex (smaller values

of Q^2 and x than in the present experiment). One is tempted to explain the observed differences in multiplicity ratios for incident hadrons and leptons as resulting from the different number and nature of the projectile constituents. However, one cannot rule out a weak dependence of the ratio on kinematic variables. It is interesting to note that our value of

TABLE III

Average values of kinematical parameters for neutrino-emulsion and neutrino-deuterium samples ($n_s^H > 2$ events only)

	No. of Events	$\langle E_{vis} \rangle$ (GeV)	$\langle E_\nu \rangle$ (GeV)	$\langle W \rangle$ (GeV)	$\langle Q^2 \rangle$ (GeV^2)	$\langle x \rangle$	$\langle y \rangle$	$\langle n_s^H \rangle$	$\langle \eta \rangle$
ν-EM	112	40.4 ±3.2	48.8 ±3.5	5.3 ±0.3	12.6 ±1.2	0.31 ±0.02	0.50 ±0.02	6.5 ±0.3	2.17 ±0.05
ν-D_2	7521	42.0 ±0.4	48.0 ±0.4	5.26 ±0.03	11.1 ±0.2	0.271 ±0.002	0.490 ±0.003	4.90 ±0.02	2.56 ±0.01

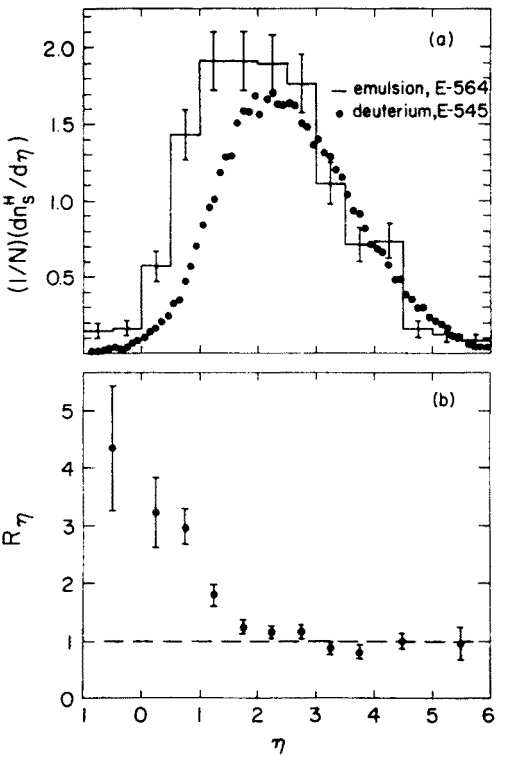

Fig. 13. (a) Comparison of laboratory-frame pseudorapidity of hadron shower tracks ($\beta \geqslant 0.7$) in ν-Em and ν-D_2 samples. N is the number of events in the respective samples, so each is normalized to one event. (b) The ratio $R(\eta)$ of the above distributions. The ν-D_2 data is from Fermilab experiment E-545 [36]. Note that the plots do not represent unbiased charged-current distributions because of the cuts on the data described in Secs. 4.3 and 4.4

R_ν is very close to the value obtained for neutrino interactions in neon [38], a lighter nucleus than the average emulsion nucleus. In the neon experiment, where the "nucleon" measurement was made indirectly by considering various charge-symmetric reactions, it was also noted that the inclusive distributions of hadrons produced in ν-Ne ($3 < W < 6$ GeV) and π-Ne ($\sqrt{s} = 4.4$ GeV) interactions are similar, with multiplicity ratios being equal within errors.

In Fig. 13, we present distributions of laboratory pseudorapidity, η, for hadrons produced with $\beta \geq 0.7$ in the two samples, and also present the ratio of the two distributions. Peaking of this ratio at low η and a fall to or below 1 at large η is qualitatively what one expects from a variety of models [27–35] and has indeed been observed in heavy-nuclear interactions of hadrons [39, 40, 41], muons [2], and neutrinos [38].

A more detailed study of nuclear effects is in preparation.

5. Decay search and analysis

All neutrino interaction candidates were scanned for evidence of short lived decays. Particular attention was given to the energetic events with an obvious mismatch between the tracks present at the primary vertex in emulsion and the tracks observed in the bubble chamber.

5.1. Decay search statistics

The decay search was carried out in two stages. To look for charged decays, all shower tracks with both azimuth and dip angles of less than 30 degrees were followed for a distance of at least 3 mm downstream from the primary vertex. For any track unmatched in the bubble chamber, the track was followed until it exited from emulsion. In the total followed track length of 1400 cm, 34 secondary vertices and 10 kinks were found, corresponding to a nuclear interaction length of 34 ± 5 cm, in good agreement with the pion mean free path in emulsion [39]. Three decay candidates are described below.

To search for neutral decays, the emulsion was double scanned at high magnification using the volume-scanning method, at least within a 30-degree half-angle cone extending $\sim$ 1 mm downstream from the primary vertex. About 50% of the events were scanned over a larger area for a total scanned area of 280 mm^2. On the average, 1 e^+e^- pair (event unassociated) was observed per 2 mm^2, with an efficiency of 80%. In addition, for a subsample, a neutral-decay search was performed by the track-following method described in Sec. 3.4. Two out of the three found neutral-decay candidates are described below. The third candidate required at least two missing neutrals, precluding definitive analysis; furthermore, it was rejected from the final charged-current sample by the muon p_t cut.

5.2. Charm decay candidates

The relevant parameters of the decay candidates considered here are summarized in Table IV. A brief description of each event (labelled with the event number and the most probable decay mode interpretation) is presented here.

TABLE IV(a)

Decay candidates — primary vertex

Event	E_{vis} (GeV)	E_ν (GeV)	x	y	W (GeV)	Q^2 (GeV/c)^2	P_μ (GeV/c)
19/1844/1134	14.6	20.8	0.16	0.45	4.0	2.9	11.4
22/1828/645	20.4	25.0	0.55	0.56	3.6	14.6	11.0
7/2221/1253	37.4	46.5	0.49	0.62	5.3	26.4	17.8
11/2071/2056	58.7	64.8	0.08	0.18	4.6	1.9	52.9
15/2185/833	95.1	98.1	0.48	0.71	8.3	64.2	28.2

TABLE IV(b)

Decay candidates — secondary vertex

Event	Decay		P_c (GeV/c)	Lifetime (10^{-13} sec)	Decay mode
	dist (μm)	angle (deg)			
19/1844/1134	50	26.7	2.37	1.4	$F^+ \to \pi^+\pi^+\pi^-\pi^0$
22/1828/645	2	17.8	3.79	0.04	$\Lambda_c^+ \to pK^-\pi^+$
7/2221/1253	1545	5.5	15.0	6.4	$D^+ \to K^-\pi^+e^+(\nu)$
11/2071/2056	422	9.8	5.9	4.4	$D^0 \to K^-\pi^+(\pi^0)$
15/2185/833	12	5.7	11.9	0.06	$D^0 \to \pi^+\pi^-(K^0)$

Event 19/1844/1134 $F^+ \to \pi^+\pi^+\pi^-\pi^0$

Full details and analysis of this event have been reported elsewhere [6]. A charged decay vertex at a distance of 50 μm from the primary vertex had three charged prongs and two converting gammas. The most probable interpretation of the decay was $F^+ \to \pi^+\pi^+\pi^-\pi^0$ with a 2-C mass fit of 2017 ± 25 MeV/c^2, with a lifetime estimated at 1.4×10^{-13} sec. This result is consistent with other hybrid emulsion data [5, 9]. However, we note that recent measurements at Cornell [42] and DESY [43] yield a lower mass estimate of 1970 ± 7 MeV/c^2.

Event 22/1828/645 $\Lambda_c^+ \to pK^-\pi^+$

A coplanar trident observed very close to the primary neutrino vertex consisted of a 0.7-GeV/c p, a 2.3-GeV/c π^+ and a 0.8-GeV/c K^-. All three tracks were unambiguously identified by emulsion and bubble chamber measurements. Missing neutrals were ruled out by the coplanarity of the trident with the primary vertex, and the invariant mass was calculated to be 2281 ± 12 MeV/c^2. A precision measurement and reconstruction [44] of a possible secondary vertex was carried out, resulting in a decay length of 2.1 ± 0.7 μm. Combined with the above evidence this 3-sigma result allows an interpretation of the decay as $\Lambda_c^+ \to pK^-\pi^+$ with a decay time of 0.04×10^{-13} sec.

Event 7/2221/1253 $D^+ \rightarrow K^-\pi^+e^+(\nu)$

All primary vertex tracks except one were well matched to the bubble chamber data. The extra track decayed into a clean trident 1545 μm downstream. One of the secondaries was identified as a 1.5 GeV positron cascading in the emulsion and in the bubble chamber, thus implying a semileptonic decay mode. For a minimum number of decay products, and because no neutral strange particle decay was seen in the chamber, the second track, well-matched by a negative track of 11.3 GeV/c interacting in the bubble chamber, was assumed to be a K^- meson. Emulsion ionization measurements are consistent with this assumption. The third track, with a momentum of 2.0 GeV/c as measured in the emulsion, required a 5-degree scatter in the emulsion box wall to provide a satisfactory match to its corresponding bubble chamber track. Because of the missing neutrino only a 0-C fit was possible, with only the lower momentum solution of $D^+ \rightarrow K^-\pi^+e^+(\nu)$ resulting in an acceptable fit with a decay time of 6.44×10^{-13} sec.

Event 11/2071/2056 $D^0 \rightarrow \pi^+K^-(\pi^0)$

In this event, a clean neutral vee was found (by track following) 422 μm downstream from the primary vertex. One of the vee tracks corresponded to an interacting hadron, whereas the other track left the chamber without interacting. From the bubble chamber momentum and emulsion ionization measurements the two tracks were identified as a pion and a kaon with momenta of 3.9 GeV/c and 2.0 GeV/c. Considering only the Cabibbo -favored decay modes with a minimum number of decay products, the missing neutral would have to be a π^0. Only the lower momentum 0-C hypothesis of $D^0 \rightarrow \pi^+K^-(\pi^0)$ provided an acceptable fit with a decay time of 44.4×10^{-13} sec.

Event 15/2185/833 $D^0 \rightarrow \pi^+\pi^-(K^0)$

This very narrow neutral vee (0.3 degree opening angle) was found 12 μm from the primary vertex. The hypothesis of two separated vertices is based on an ionization gap probability of 2×10^{-4} and on an accurate geometrical reconstruction in which at least one of the vee tracks misses the primary vertex at the 85% confidence level [45]. One of the two tracks was a well-matched 8-GeV/c positive hadron. The other track, also a hadron, interacted only 4 cm into the bubble chamber liquid, placing only a lower limit on its momentum. A negative charge for this track is the favored hypothesis because it yields better agreement between extrapolated and measured angles in the emulsion. From emulsion ionization and bubble chamber momentum measurements the positive track was identified as a pion. From ionization and multiple scattering measurements in the emulsion, the negative track was identified as a 2.5 GeV/c pion. No evidence of strange decays into two charged particles was observed in the bubble chamber. The momentum imbalance at the secondary vertex was 0.32 ± 0.27 GeV/c. The invariant mass of the pair of 0.33 ± 0.02 GeV/c^2, along with the very short decay length, preclude an interpretation as $K^0 \rightarrow \pi^+\pi^-$. Because of missing neutral(s), a 0-C fit was possible only for the preferred interpretation of this event as $D^0 \rightarrow \pi^+\pi^-$ (K^0) with a decay time of 0.06×10^{-13} sec.

We conclude this section by estimating the charm-production cross section relative to the charged-current neutrino cross section in emulsion. We obtain a value of $4\pm2\%$ where the error is purely statistical for our sample of 128 charged-current events, consistent with a higher-statistics result of $6.5\pm1.9\%$ [5, 9].

6. *Conclusions*

The unique feature of this experiment was the exposure of emulsion stacks inside a bubble chamber in an attempt to utilize the chamber's potential as a downstream particle detector and analyzer for a study of short-lived decays.

A total of 128 charged-current neutrino interactions were located in the emulsion. Five of these events could be interpreted as containing charm particle decays. The masses and/or lifetimes were found to be consistent with published values.

A comparison between emulsion and deuterium data was carried out in a preliminary study of nuclear effects. Pseudorapidity distributions of the produced hadrons were found to be different in the target fragmentation region. The overall multiplicity ratio was $R_\nu = 1.32\pm0.05$.

We wish to thank the Fermilab 15-foot Bubble Chamber crew for their help in installing our emulsions in the chamber and for the successful operation of the chamber during our run. We are grateful to the scanning and measuring staffs of our various laboratories for their patience and diligence in finding and measuring events not only in complicated bubble chamber topologies, but in emulsions as well. We are indebted to the late Dr. K. Bogomolov for producing our emulsions, and to Dr. N. Lubomilov for processing them. We thank the IIT-Maryland-Stony Brook-Tohoku-Tufts (E-545) and BNL-Columbia--Rutgers (E-53) Collaborations for making the bubble chamber film available to us for analysis and copying. We are particularly grateful to the E-545 Collaboration for allowing us access to their DST to make the emulsion-deuterium comparisons of Section 4.5, and for their permission to publish selections of their data in Figures 10–13.

This work was supported in part by the U. S. Department of Energy and the U. S. National Science Foundation.

REFERENCES

[1] E. H. S. Burhop et al., *Phys. Lett.* **65B**, 299 (1976); A. L. Read et al., *Phys. Rev.* **D19**, 1287 (1979).
[2] L. Hand et al., *Acta Phys. Pol.* **B9**, 1087 (1978); L. Hand et al., *Z. Physik* **C1**, 139 (1979).
[3] V. I. Baranov et al., *Sov. J. Nucl. Phys.* **39**, 1425 (1984).
[4] D. Allasia et al., *Nucl. Phys.* **B176**, 13 (1980).
[5] K. Niu, Proceedings of the XX-th International Conference on High Energy Physics, Madison, USA, 1980, Vol. 1, p. 352; N. Ushida et al., *Phys. Rev. Lett.* **45**, 1043 (1980); **45**, 1053 (1980); **48**, 844 (1982); **51**, 2362 (1983); N. Ushida et al., *Phys. Lett.* **121B**, 287, 291 (1983).
[6] R. Ammar et al., *Phys. Lett.* **94B**, 118 (1980).
[7] M. Adamovich et al., *Phys. Lett.* **99B**, 271 (1981).
[8] R. L. Rosenbladt, University of Washington Preprint VTL-PUB-77 (1981).
[9] S. M. Errede, Ph. D. Thesis, Ohio State University, Columbus, USA, 1981; M. J. Gutzwiller,

Ph. D. Thesis, Ohio State University, Columbus, USA, 1981; D. C. Bailey, Ph. D. Thesis, McGill University, Montreal, Canada, 1983.
[10] J. Sandweiss et al., *Phys. Rev. Lett.* **44**, 1104 (1980).
[11] L. Foa, Proceedings of the X-th International Symposium on Lepton and Photon Interactions, Bonn 1981, p. 775.
[12] W. Allison et al., *Phys. Lett.* **93B**, 509 (1980); B. Adeva et al., *Phys. Lett.* **102B**, 285 (1981).
[13] E. Albini et al., *Phys. Lett.* **110B**, 339 (1982).
[14] M. J. Murtaugh, Proceedings of the 1979 International Symposium on Lepton and Photon Interactions, Batavia 1979, p. 277; H. E. Fisk, Proceedings of the X-th International Symposium on Lepton and Photon Interactions, Bonn 1981, p. 703; V. V. Ammosov et al., *Nucl. Phys.* **B177**, 365 (1981).
[15] C. S. Bogomolov et al., 1st International Conference on Nuclear Photography, Strasbourg 1958, p. 203; C. S. Bogomolov et al., Proceedings of the 10th International Conference on Solid State Nuclear Track Detectors, Lyon, H. Francois et al., eds., Pergamon, New York 1980, p. 127; V. I. Baranov et al., IHEP Preprint 83-190 (1983).
[16] F. Solmitz, A. Johnson, T. E. Day, *Three View Geometry Program*, Univ. of California — LBL, Alvarez Group Programming Note P-117, June 20, 1966.
[17] Hydra Application Library, CERN, 1974.
[18] E. A. Slobodyuk, *EMPRED Long Write-Up*, E-564 Internal Report, February 8, 1982; S. Krzywdzinski, H. A. Rubin, *EMPRD Corrections*, University of Washington Note VTL-PN-194 (1984).
[19] P. Goritchev et al., ITEP-33 Preprint (1982); V. Ammosov et al., IHEP-71 Preprint (1984).
[20] J. Babecki et al., *Acta Phys. Pol.* **B9**, 495 (1978).
[21] J. W. Chapman et al., *Phys. Rev.* **D14**, 5 (1976).
[22] J. Hanlon et al., *Phys. Rev. Lett.* **45**, 1817 (1980); T. Kitagaki et al., *Phys. Rev. Lett.* **49**, 98 (1982).
[23] S. Barish et al., *Phys. Rev.* **D18**, 2217 (1978).
[24] H. G. Heilmann, University of Bonn, Internal Report No. WA-21-Int-1 (1978) unpublished; J. Bleitschau et al., *Phys. Lett.* **87B**, 281 (1978).
[25] A. Grant, *Nucl. Instrum. Methods* **127**, 355 (1975).
[26] A. Białas, W. Czyż, *Nucl. Phys.* **B137**, 359 (1978).
[27] S. Brodsky et al., *Phys. Rev. Lett.* **39**, 1120 (1977).
[28] Y. Afek et al., *Phys. Rev.* **D15**, 2622 (1977).
[29] G. Davidenko, N. Nikolaev, *Nucl. Phys.* **B135**, 333 (1978).
[30] G. Nilsson, B. Anderson, G. Gustafson, *Phys. Lett.* **83B**, 379 (1979).
[31] M. Hossain, D. Tow, *Phys. Rev.* **D21**, 1842 (1980).
[32] M. Nikolaev, *Z. Physik* **C5**, 291 (1980).
[33] A. Dar, F. Takagi, *Phys. Rev. Lett.* **44**, 768 (1980).
[34] A. Dar, Technion-PH-80-26, Preprint (1980).
[35] A. Białas, E. Białas, *Phys. Rev.* **D21**, 675 (1980); A. Białas, *Acta Phys. Pol.* **B11**, 475 (1980).
[36] Private Communication from the Fermilab E-545 Collaboration: IIT, University of Maryland, the State University of New York at Stony Brook, Tohoku University, and Tufts University.
[37] J. Babecki, *Acta Phys. Pol.* **B6**, 443 (1975).
[38] T. H. Burnett et al., *Phys. Lett.* **77B**, 443 (1978).
[39] E. V. Anzon et al., *Phys. Lett.* **31B**, 237 (1970)
[40] M. V. Lee, J. J. Lord, R. J. Wilkes, *Phys. Rev.* **D19**, 55 (1979).
[41] C. De Marzo et al., *Phys. Rev.* **D26**, 1019 (1982).
[42] A. Chen et al., *Phys. Rev. Lett.* **51**, 634 (1983).
[43] H. Albrecht et al., (ARGUS-DESY), *Phys. Lett.*, to be published.
[44] S. A. Bunyatov et al., JINR-Dubna preprint D1-82-447 (1982).
[45] V. Shamanov, ITEP-74 Preprint (1984).